On the Application of Complex Resistive Boundary Conditions to Model Transmission Lines Consisting of Very Thin Superconductors

JEFFREY M. POND, MEMBER, IEEE, CLIFFORD M. KROWNE, SENIOR MEMBER, IEEE, AND WILLIAM L. CARTER

Abstract—**A resistive boundary condition for the case where the resistivity is assumed to be a complex quantity is shown to be an accurate model for a superconducting film which is thin compared to the superconducting penetration depth. The imaginary part of the conductivity is the dominant term and is a measure of the inductive energy stored in the superconductor. Numerical solutions of superconducting microstrip have been obtained and are compared to experimental results and to analytic solutions for superconducting parallel-plate waveguides. Excellent agreement has been found between experimental, analytical, and numerical results.**

I. INTRODUCTION

TRANSMISSION lines using superconducting films have many possible practical applications in microwave and millimeter-wave devices and circuits [1]. The advantages of superconducting transmission lines include low loss and low dispersion. In addition, superconducting microstrip can be made very small if the geometry is chosen to give a very slow phase velocity. The very slow phase velocity is the result of the inductance contribution from the energy stored in the superconductor, called the kinetic inductance (L_k). The energy is stored as the kinetic motion of the charge carriers in the superconductor. The slowing of an electromagnetic wave on a superconducting transmission line due to the contribution of L_k was pointed out by Pippard in 1947 [2]. Microstrip lines in which L_k is much larger than the magnetic inductance (L_m) have been fabricated [3], [4] and found to have dielectric-limited loss and very slow phase velocities. Very compact broad-band microwave devices and circuits such as tunable phase shifters, filters, and delay lines can be realized using these microstrip lines.

The measurement of this slow-wave behavior has been used to determine the penetration depth, λ, of superconducting films [5]. The penetration depth is the characteristic decay length of a magnetic field into a superconductor. In order to achieve the very slow phase velocities reported in [3] and [4] the superconducting film thicknesses must be much thinner than λ. In contrast to more conventional geometries, this implies that the superconducting film is diaphanous, meaning that the electromagnetic field on one side of the film is determined by the film properties, the geometry, and the electromagnetic field on the other side of the film. Such field penetration in superconductors has been studied analytically [6] and observed experimentally [7] for the case of Josephson junctions inductively coupled to microstrip. Significant coupling of electromagnetic energy through superconducting films has been measured even when the film thickness is as great as the penetration depth. This field penetration obviously complicates the solution of any electromagnetic problem, since a three-region problem must always be solved for each superconducting film. Properties of a thin superconducting film, thin meaning that the thickness is much less than λ, can be accounted for by a complex conductivity. Thus, as will be shown in the next section, it is possible to model these very thin superconducting films by using the resistive boundary condition [8]. The resistive boundary condition allows a reduction in the complexity of the problem being solved, from a three-region problem with field matching at two interfaces to a two-region problem with a new field matching condition, determined by the film properties, at one interface. The conductivity of the layer, rather than representing only a loss term, is a complex quantity where the real part corresponds to the conductivity of the normal electrons (in the two-fluid model) or quasiparticles (in BCS theory). Thus, the real part of the conductivity represents the energy loss in the film. The imaginary part of the conductivity is related directly to the superfluid (in the two-fluid model) or Cooper pair (in BCS theory) component of the current. The imaginary component is determined by λ and represents the inductive energy stored within the film.

There is always a small amount of energy stored within any conductor, but only for superconductors can a significant proportion of the energy be stored this way without

Manuscript received February 17, 1988; revised June 6, 1988. This work was supported by the Office of Naval Research.

J. M. Pond and C. M. Krowne are with the Microwave Technology Branch, Electronics Science and Technology Division, Naval Research Laboratory, Washington, DC 20375-5000.

W. L. Carter is with American Semiconductor, Cambridge, MA.

IEEE Log Number 8823697.

incurring losses which would be prohibitive in a transmission line structure. This can most easily be seen by applying the two-fluid model [9] to a conductor of unit length with a cross-sectional area A. In the simplest case [10], the conductance is

$$G = n_n e^2 A\tau/m \tag{1}$$

and the dominant inductive susceptance is

$$1/(\omega L_k) = n_{sc} e^2 A/m\omega \tag{2}$$

where m, e, and τ are the mass, charge, and collision time of an electron. The densities of the normal and superconducting electrons are given by n_n and n_{sc}, respectively. The normal and the superconducting electrons act as parallel conduction mechanisms. Since $n_{sc}/\omega \gg n_n\tau$, except for temperatures very close to the critical temperature (T_c), the susceptance is larger than the conductance. In the normal state $n_s = 0$ and the inductive susceptance, using the Drude model [9], is given by

$$1/(\omega L_k) = n_n e^2 A\tau(\omega\tau)/m. \tag{3}$$

Since for microwave frequencies $\omega\tau \ll 1$, it is obvious that the energy stored will greatly exceed the energy lost only in the superconducting state.

This paper demonstrates the application of the resistive boundary condition to solve for the propagation constant for the case of two parallel sheets described by complex resistive boundary conditions. Solutions for electromagnetic propagation in a trilayer consisting of a lossy dielectric between two superconducting films have been presented for both the simple two-fluid model [11] and the Mattis–Bardeen theory for complex conductivity [12]. The solutions derived using the resistive boundary condition are shown to be equivalent, as they must be, to the solution for the arbitrary thickness case in the limit where the film thickness is less than λ. The motivation for introducing the resistive boundary condition, however, is not to solve a configuration for which a solution already exists. Rather, the purpose is to introduce a technique which can be applied in a numerical formulation of transmission line structures for which closed-form solutions are not tractable and for which existing numerical approaches are inadequate.

From a practical viewpoint, microstrip, slotline, coplanar strip, and coplanar waveguide are the transmission structures of interest. Traditional numerical approaches [13]–[16] to these structures are not easily applied to very thin superconductors due to the coupling of the fields which can exist from one side of the superconducting film to the other. A new formulation, based on a generalization of the spectral-domain method [15] for the solution of transmission line structures, is presented. A numerical formulation which has been implemented to solve for a microstrip transmission line structure is then discussed.

The results of the microstrip numerical solution for the complex resistive boundary condition are compared with the analytical solution for a superconducting parallel-plate waveguide and with experimental results. The agreement between the analytical predictions for the parallel-plate case and the measured values for the microstrip is excellent, as has been discussed earlier [4]. A comparison of these results with the numerical results using the complex resistive boundary condition is used to establish the validity of this application of the boundary condition and the numerical formulation. Thus, this technique can be used to investigate a wide variety of practical transmission line structures where thin superconducting films are practical but neither conventional analytic approaches nor traditional numerical formulations are applicable. In particular, the formalism can be used to determine the propagation properties of slotline, coplanar strip, and coplanar waveguide.

II. Theory

The macroscopic theory of electromagnetic fields in superconductors is well understood [9], [17] and can be related to simple macroscopic properties. In the short presentation to follow, it is assumed that the two-fluid model and the London equations are valid. This means that the electromagnetic properties of a superconductor can be accounted for by a temperature-dependent complex conductivity. Other expressions for a complex conductivity, based on BCS theory, are available and are discussed in the Appendix. The BCS derived expressions are theoretically based rather than phenomenologically based and are applicable to both local and nonlocal superconductors. For local superconductors and even many nonlocal superconductors, however, the two-fluid description is usually adequate. In particular, the experimental results to be presented later are for microstrip lines fabricated from niobium nitride (NbN), which is a local superconductor.

The current in a superconductor, according to the two-fluid model, can be written as

$$\boldsymbol{J} = \boldsymbol{J}_n + \boldsymbol{J}_{sc} \tag{4}$$

where $\boldsymbol{J}_n$ is the current due to the normal electrons and $\boldsymbol{J}_{sc}$ is the current due to the superconducting electrons. Ohm's law applies to the normal electrons,

$$\boldsymbol{J}_n = \sigma_n \boldsymbol{E} \tag{5}$$

while $\boldsymbol{J}_{sc}$ is governed by the London equations,

$$\frac{\partial \boldsymbol{J}_{sc}}{\partial t} = \frac{\boldsymbol{E}}{\mu_0 \lambda^2} \tag{6}$$

and

$$\nabla \times \boldsymbol{J}_{sc} = -\frac{\boldsymbol{H}}{\lambda^2}. \tag{7}$$

Assuming an $e^{j\omega t}$ time dependence, the Maxwell equations and London equations yield a wave equation,

$$\nabla^2 \boldsymbol{H} = \left(\lambda^{-2} + j\omega\mu_0\sigma_n - \omega^2\mu_0\epsilon\right)\boldsymbol{H}. \tag{8}$$

Thus a complex conductivity can be defined:

$$\sigma = \sigma_n - j\sigma_{sc} \tag{9}$$

where

$$\sigma_{sc} = \left(\omega\mu_0\lambda^2\right)^{-1}. \tag{10}$$

The Appendix discusses the two-fluid model as well as other models of complex conductivity for superconductors. However, irrespective of the conductivity model used, (8) can be applied to describe the electromagnetic properties of a superconductor.

The resistive boundary condition [8] is an approximate boundary condition in electromagnetic theory. It has been used to treat thin lossy dielectric sheets with large conductivities where the thickness (t) is much less than a wavelength. The resistance, in Ω/square, of such a sheet is given by

$$R = 1/\sigma t. \tag{11}$$

Solving the electromagnetic field problem for such a sheet can be reduced from a problem of matching fields at two surfaces to matching fields at one surface if it is assumed that

$$\lim_{\substack{t \to 0 \\ \sigma \to \infty}} \frac{1}{\sigma t} = R. \tag{12}$$

Using the notation that + and − superscripts refer to the field components of $\boldsymbol{E}$ and $\boldsymbol{H}$ on, respectively, the top and the bottom of the resistive sheet, the boundary conditions for the electromagnetic field become

$$\hat{n} \times (\boldsymbol{E}^+ - \boldsymbol{E}^-) = 0 \tag{13}$$

$$\hat{n} \times (\boldsymbol{H}^+ - \boldsymbol{H}^-) = \boldsymbol{J}_s = -(1/R)\hat{n} \times (\hat{n} \times \boldsymbol{E}^{\pm}) \tag{14}$$

where $\hat{n}$ is a unique unit normal vector to the resistive interface.

In the case of a superconducting thin film where the film thickness, t_{sc}, is small compared to the characteristic penetration lengths in both the normal and the superconducting state, the use of this approximate boundary condition is valid. Specifically, the cases of interest are those for which $t \ll \lambda$ and $t \ll \delta$, where δ is the classical skin depth, given by

$$\delta = [2/(\omega \mu_0 \sigma_n)]^{1/2}. \tag{15}$$

Thus, the surface resistance is given by

$$R = [t_{sc}(\sigma_n - j\sigma_{sc})]^{-1}. \tag{16}$$

Even though the resistivity is now a complex quantity, it will still be referred to as a complex resistive boundary condition, since the term *impedance boundary condition* refers to an entirely different boundary condition [8]. To demonstrate the applicability of this technique to a simple but useful and instructive case, the analytic solution to a parallel-plate transmission line structure will be presented in the following section.

III. Parallel-Plate Transmission Line

In the following discussion all resistive boundary conditions, R_i, are assumed to have an imaginary part, $\mathrm{Im}(R_i)$, which is much larger in magnitude than the real part, $\mathrm{Re}(R_i)$. The parallel-plate structure, shown in Fig. 1, consists of two resistive boundary conditions, R_1 at $x = d/2$ and R_3 at $x = -d/2$, and is assumed to have an

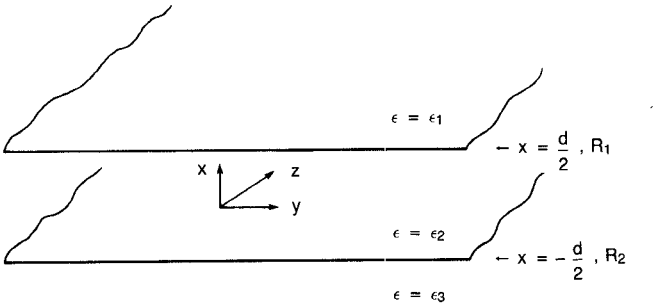

Fig. 1. Parallel-plate transmission line with resistive boundary conditions, R_1 and R_3, separating dielectric regions ϵ_1 and ϵ_2 at $x = d/2$ and dielectric regions ϵ_2 and ϵ_3 at $x = -d/2$, respectively. Field quantities were assumed to be functionally independent of y and to be propagating in the z direction.

electromagnetic wave propagating in the positive z direction of the form $e^{j(\omega t - az)}$ with $\mathrm{Re}(a) > 0$ and $\mathrm{Im}(a) < 0$. All field components are assumed to be independent of the y direction. A TM solution will be assumed, i.e., $H_x = H_z = E_y = J_y = 0$. Thus the parallel-plate solution derived will have a field pattern closely approximating a very wide microstrip or suspended stripline. The half-space $x > d/2$ is described by ϵ_1 and μ_0, and the half-space $x < -d/2$ is described by ϵ_3 and μ_0. The region between the sheets is described by μ_0 and ϵ_2. Since the resistive boundary conditions are penetrable, it will be assumed that $\epsilon_2 > \epsilon_1$ and $\epsilon_2 > \epsilon_3$. This ensures that the fundamental mode is primarily between the plates. Components of the electromagnetic field which can exist in each of the regions ($i = 1,2,3$) are given by [11]

$$E_x = C_i^+ e^{k_i x} + C_i^- e^{-k_i x} \tag{17}$$

$$E_z = -(jk_i/a)C_i^+ e^{k_i x} + (jk_i/a)C_i^- e^{-k_i x} \tag{18}$$

$$H_y = (a^2 - k^2)/(a\omega\mu_0)E_x \tag{19}$$

where in each region

$$k_i^2 = a^2 - \omega^2 \mu_0 \epsilon_i, \qquad i = 1,2,3. \tag{20}$$

The unknown complex constants, C_i^- and C_i^+, are determined by matching the fields. The value of k_i is assumed to be the root given by (20), which has a positive real part. In regions 1 and 3 only C_1^- and C_3^+, respectively, can exist if the fields are to be finite. Thus, there exist four unknown coefficients and two boundary conditions given by (13) and (14) to be imposed at each resistive boundary. Solving the four equations simultaneously gives a transcendental equation for a, which is given by

$$(f_1 + f_3)g_2 \cosh(k_2 d) + (g_2^2 + f_1 f_3)\sinh(k_2 d) = 0 \tag{21}$$

where

$$f_i = g_i - j\omega\mu_0/R_i, \qquad i = 1,3 \tag{22}$$

$$g_i = (a^2 - k_i^2)/k_i, \qquad i = 1,2,3. \tag{23}$$

To solve for the fundamental mode, the only mode to be discussed in this paper, an approximate expression can be derived which yields very accurate results for very wide microstrip. For the fundamental mode, $k_2 d \ll 1$. Further-

more, under situations for which

$$|\omega\mu_0/R_i| \gg |g_i|, \qquad i=1,3 \tag{24}$$

$$\left|(\omega\mu_0)^2/(R_1R_3)\right| \gg |g_2|^2 \tag{25}$$

(21) reduces to an equation for a which is given by

$$a^2 = \omega^2\mu_0\epsilon_2\left[1 - j(R_1/\omega\mu_0 d) - j(R_3\omega\mu_0 d)\right]. \tag{26}$$

If it is further assumed that $\sigma_{sc} \gg \sigma_n$, then a is approximately given by

$$a^2 = \omega^2\mu_0\epsilon_2\left[1 + \lambda_1^2/dt_1 + \lambda_2^2/dt_2\right] \tag{27}$$

where λ_1 and λ_2 refer to the penetration depths of the films at $x = d/2$ and $x = -d/2$, respectively. The thicknesses of these films are t_1 and t_2, respectively. It should be noted that a increases rapidly as $T \to T_c$, due to the strong temperature dependence of λ, given in (A1).

The expression for a given by (26) is independent of both ϵ_1 and ϵ_3. This implies that, in the reduction of a to the approximate form, the fields in the exterior dielectric regions become negligible. This is a result of the special nature of this particular one-dimensional problem in the limits investigated, and is not generally true for superconducting films which are thinner than a penetration depth. In fact, analytical results [6] for two parallel-plate structures with one common thin plate show that significant coupling through the common plate can occur if the plate is thinner than a penetration depth. Recently, experimental measurements have been made [7] which confirm coupling through thin films arranged in this way.

It is now possible to show that the approximations which lead to (26) are valid for situations of practical interest. The assumption that $k_2 d \ll 1$ leads, using (20) and (27), to an upper frequency limit given by

$$\omega \ll \frac{c_2}{d\left[\left(\lambda_1^2/dt_1\right) + \left(\lambda_2^2/dt_2\right)\right]^{1/2}} \tag{28}$$

where c_2 is the speed of light in an infinite medium of ϵ_2. It is now easy to show that (24) and (25) are valid for the derivative of (26). Noting that $\epsilon_2 > \epsilon_1$ and $\epsilon_2 > \epsilon_3$, it follows that if

$$|\omega\mu_0/R_i| \gg |g_2|, \qquad i=1,3 \tag{29}$$

then (24) and (25) are also satisfied since $|g_2| > |g_1|$ and $|g_2| > |g_3|$. Using (20) and (27), the relationship in (24) can be written as

$$t_i/\lambda_i^2 \gg (\omega/c_2)\left[\lambda_1^2/(dt_1) + \lambda_2^2/(dt_2)\right]^{-1/2}, \qquad i=1,2. \tag{30}$$

The relationship for an upper frequency limit given by (28) can now be applied. Hence, (30) can be written as

$$t_i/\lambda_i^2 > \frac{t_i}{\lambda_i^2\left[1 + \left(\lambda_j^2 t_i\right)/\left(\lambda_i^2 t_j\right)\right]},$$

$$i=1,2;\ j = \begin{cases} 2 & \text{if } i=1 \\ 1 & \text{if } i=2 \end{cases} \tag{31}$$

which is obviously true for all real values. Thus, all approximations made to arrive at the closed-form expression of (26) are valid provided that the frequency is small enough to satisfy (28).

This problem has also been solved for superconducting layers of arbitrary thickness [11], [12], [17]. Hence, the solution presented above is a limiting case of existing expressions. The solution for superconducting films of arbitrary thickness is given by

$$a^2 = \omega^2\mu_0\epsilon_2\left[1 + (\lambda_1/d)\coth(t_1/\lambda_1) + (\lambda_2/d)\coth(t_2/\lambda_2)\right]. \tag{32}$$

If $t/\lambda < 1$ then $\coth(t/\lambda) \cong \lambda/t$ and consequently (32) reduces to the expression just derived using the complex resistive boundary condition. Furthermore, the frequency limitation given by (28) is the same as the one given in [11] under the same thin-film limit.

The losses in the transmission line can come from two sources: the dielectric loss and the superconductor loss. The dielectric losses are related directly to the dielectric loss tangent of the dielectric layer between the superconducting films. For small values of the dielectric loss tangent and assuming that the superconductor losses are zero, (27) gives

$$\mathrm{Im}(a) = \frac{\omega}{a}\left(\mu_0\mathrm{Re}(\epsilon_2)\right)^{1/2}\left[1 + \frac{\lambda_1^2}{dt_1} + \frac{\lambda_2^2}{dt_2}\right]^{1/2} \cdot \left[\mathrm{Im}(\epsilon_2)/\mathrm{Re}(\epsilon_2)\right]. \tag{33}$$

The superconductor losses can also be determined from (26) assuming that the losses are small and the dielectric losses are zero. Using (26) and assuming $\sigma_{1sc} \gg \sigma_{1n}$ and $\sigma_{2sc} \gg \sigma_{2n}$, the dominant term of the imaginary part of a is found to be

$$\mathrm{Im}(a) = -\left[\omega^2/(2d)\right](\mu_0\epsilon_2)^{1/2} \cdot \frac{\mu_0\sigma_{1n}\lambda_1^4/t_1 + \mu_0\sigma_{2n}\lambda_2^4/t_2}{\left[1 + \lambda_1^2/(dt_1) + \lambda_2^2/(dt_2)\right]^{1/2}}. \tag{34}$$

These expressions ((33) and (34)) agree with earlier expressions [11] if $\lambda_i \gg t_i$ $(i=1,2)$. These expressions show a very strong dependence on T as T_c is approached.

IV. Microstrip and Stripline

The microstrip geometry shown in Fig. 2 can be solved using a modified spectral-domain immittance [13] approach based on the transverse resonance method. After developing the appropriate equations to account for the complex resistive boundary condition, the numerical results for the geometry shown in Fig. 2 will be compared to the results for the infinitely wide parallel-plate case, which was presented in the previous section.

The general formulation [18] begins with the description of the electric field, $\boldsymbol{E}$, given in terms of a dyadic impedance Green's function, $\overline{\overline{Z}}$, and the currents, $\boldsymbol{J}$. Hence $\boldsymbol{E}$ is given by

$$\boldsymbol{E}(\boldsymbol{r}) = \int_v \overline{\overline{Z}}(\boldsymbol{r}, \boldsymbol{r}') \cdot \boldsymbol{J}(\boldsymbol{r}')\, dv' \tag{35}$$

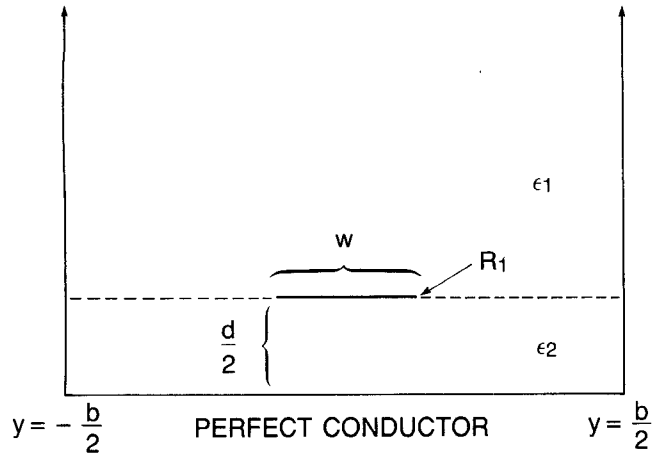

Fig. 2. Geometry of the problem which was numerically implemented. A finite width (w) strip with a resistive boundary condition, R_1, is separated from a perfectly conducting ground plane by a dielectric, ϵ_2, of thickness $d/2$.

where the integral is over the currents in the strip. The dyadic Green's function, $\bar{\bar{Z}}(\boldsymbol{r}, \boldsymbol{r}')$, describes the dielectric layer structure and also takes into account the perfectly conducting ground plane. Since the structure is infinite in the propagation direction, z, the electric field at the strip interface, from (35), reduces to

$$\boldsymbol{E}(y) = \int_{-w/2}^{w/2} \bar{\bar{Z}}(y, y') \cdot \boldsymbol{J}_s(y')\, dy' \tag{36}$$

where $\boldsymbol{J}_s(y)$ is the vector surface current. A generalization of earlier work [13] must now be made to account for the boundary condition on the strip. Using (13) and (14) for the values of the tangential electric field on the strip, two coupled equations for the surface currents, $J_{sx}(y)$ and $J_{sz}(y)$, can be derived from (36) for $-w/2 < y < w/2$ and are given by

$$\int_{-w/2}^{w/2} \left[Z_{yy}(y, y') J_{sy}(y') + Z_{yz}(y, y') J_{sz}(y') \right] dy' = E_y(y) = R J_{sy}(y) \tag{37}$$

and

$$\int_{-w/2}^{w/2} \left[Z_{zy}(y, y') J_{sy}(y') + Z_{zz}(y, y') J_{sz}(y') \right] dy' = E_z(y) = R J_{sz}(y). \tag{38}$$

A one-dimensional Fourier transform is defined as

$$\tilde{A}(\zeta) = \int_{-\infty}^{\infty} A(y) e^{-j\zeta y}\, dy \tag{39}$$

where the $\sim$ over a variable denotes the Fourier transform of that variable without the $\sim$. Since the current components are identically zero for $y < -w/2$ and $y > w/2$, the left-hand sides of (37) and (38) present no problems in performing the Fourier transforms. For the right-hand sides it should be noted that the electric field is nonzero everywhere. The tangential components of the electric field on the plane $x = 0$ are defined as

$$E_{z0} = E_{z0}^s + E_{z0}^e \tag{40}$$

and

$$E_{y0} = E_{y0}^s + E_{y0}^e \tag{41}$$

where

$$E_{\alpha 0}^s = \begin{cases} E_\alpha, & -w/2 < y < w/2 \\ 0, & y < -w/2 \text{ and } y > w/2 \end{cases} \qquad \alpha = y, z \tag{42}$$

and

$$E_{\alpha 0}^e = \begin{cases} 0, & -w/2 < y < w/2 \\ E_\alpha, & y < -w/2 \text{ and } y > w/2 \end{cases} \qquad \alpha = y, z. \tag{43}$$

Therefore, the Fourier transforms of (37) and (38) are given by

$$\left[\tilde{Z}_{yy}(\zeta) - R \right] \tilde{J}_{sy}(\zeta) + \tilde{Z}_{yz}(\zeta) \tilde{J}_{sz}(\zeta) = \tilde{E}_y^e(\zeta) \tag{44}$$

$$\tilde{Z}_{zy}(\zeta) \tilde{J}_{sy}(\zeta) + \left[\tilde{Z}_{zz}(\zeta) - R \right] \tilde{J}_{sz}(\zeta) = \tilde{E}_z^e(\zeta). \tag{45}$$

The forms of (44) and (45) are identical to previous formulations if R is identically zero. Thus, by modifying the Fourier-transformed impedance Green's functions so that $\tilde{Z}_{yy}(\zeta)$ and $\tilde{Z}_{zz}(\zeta)$ are replaced by $\tilde{Z}_{yy}(\zeta) - R$ and $\tilde{Z}_{zz}(\zeta) - R$, respectively, the problems of interest can be solved using established numerical techniques.

The elements of the dyadic impedance Green's function in the transform domain are determined using the spectral-domain immittance approach [14]. The currents are expanded in a set of basis functions [16] under the assumption that perfect electric walls exist at $y = \pm b/2$ such that

$$J_{sz}(y) = \left(1 - (2y/w)^2\right)^{-1/2} \sum_{m=0}^{m_z} a_m \cos(2m\pi y/w), \qquad 0 \leqslant y \leqslant w/2 \tag{46}$$

$$J_{sy}(y) = \left(1 - (2y/w)^2\right)^{-1/2} \sum_{m=1}^{m_y} b_m \sin(2m\pi y/w), \qquad 0 \leqslant y \leqslant w/2 \tag{47}$$

where a_m and b_m are unknown and each term satisfies the edge condition. The Fourier transforms of (46) and (47) are then substituted into (44) and (45). A Galerkin approach [16] was used to construct a determinant equation for the unknown complex propagation constant, a. The computer code was a modified version of the computer code used in [15].

V. Experimental Measurements

Experimental results have been reported [3], [4] for microstrip lines, as shown in Fig. 3, operating in a L_k dominated regime. A short summary of the geometry, fabrication, and measured results is presented below to facilitate the comparison of the analytical and the numerical approach to the actual measured results. The devices consisted of a NbN ground plane and a NbN strip separated by a Si dielectric. A ground plane was made by RF

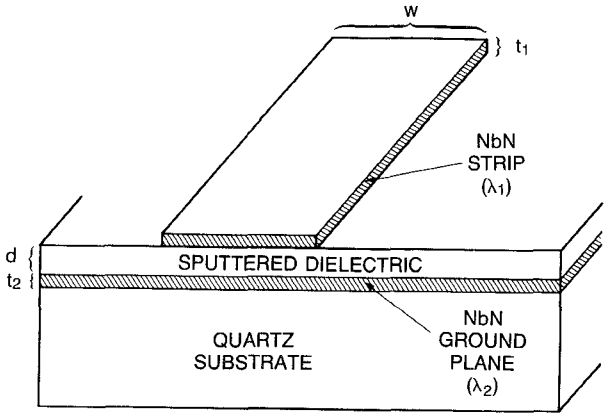

Fig. 3. Geometry of the microstrip on which experimental measurements were made.

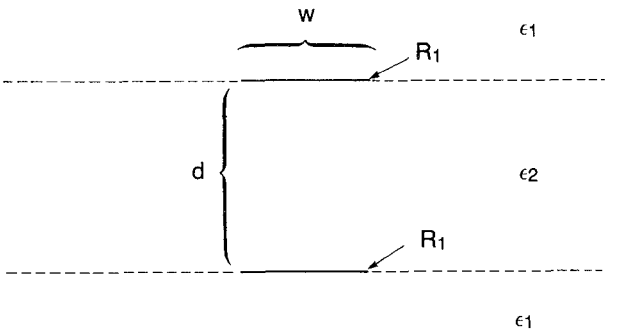

Fig. 4. Equivalent suspended stripline geometry of Fig. 2 using image theory of the perfectly conducting ground plane.

sputtering 150 Å of NbN onto a quartz substrate. The dielectric consisted of an RF-sputtered thin film of hydrogenated Si which was deposited in two steps for a total thickness of 450 Å. The strip was deposited in the same fashion as the ground plane but was only 140 Å thick. This top film was then patterned to define 25-μm-wide microstrip lines of various lengths.

Extensive time- and frequency-domain measurements have been made with these devices [3], [4] and their behavior was found to correlate very well with calculations of the parallel-plate waveguide case for superconducting layers of arbitrary thickness (32). This is not surprising, considering that the width-to-height ratio of the microstrip is over 500 and that fringing field contributions should be negligible. In particular, the temperature dependence of the propagation constant follows the behavior predicted by the two-fluid model to within the experimental accuracy. Assuming two 145 Å NbN films, the parameters of the lines were determined to be $T_c = 12.15$ K, $\lambda_0 = 3200$ Å, and $\epsilon_{Si} = 10.5$. These values were derived during earlier work [4], where a best fit of the measured response as a function of frequency and temperature was made to a circuit model. They are all reasonable values for the thin sputtered films. Losses in the lines were limited by the dielectric.

VI. Results

Correlation between analytical, numerical, and experimental results was excellent for these structures. When comparing analytical, numerical, and experimental results, it should be noted that there existed some slight differences in the geometries that were solved. The analytical results, based on (27), considered the case of an infinitely wide parallel-plate waveguide where all fields were assumed to be independent of the transverse y direction. Experimental results were obtained from the microstrip configuration shown in Fig. 3 at 0.5 and 1.0 GHz. Since the width-to-height ratio of the microstrip was greater than 500, the parallel plate was expected to provide a good approximation for the dominant mode.

The structure solved numerically was actually a different geometry from both the analytical and the experimental geometry. For the numerical solution a strip of finite width was modeled as a complex resistive boundary condition separated from a perfectly conducting ground plane by a dielectric layer as shown in Fig. 2. In order to have the numerical geometry approximate the analytical geometry, the perfectly conducting ground plane was treated as an image plane, which for a very wide strip will approach the parallel-plate geometry. In addition, this geometry is easier to implement numerically than the actual microstrip configuration shown in Fig. 3. The resultant transmission line was a suspended stripline as shown in Fig. 4 with a dielectric thickness which was twice the distance between the strip and the perfectly conducting ground plane of the numerical geometry. Once again, due to the very large value of the width-to-height ratio, the approximation should be quite accurate. Of course, the characteristic impedance value would differ by a factor of two.

A comparison of the Re(a) at 1.0 GHz for the analytical, numerical, and experimental data is shown in Fig. 5 as a function of temperature for the geometries that most closely approximated the experimental case. In each situation the superconducting and dielectric film parameters mentioned in the previous section were used in the analytical and numerical models. For the numerical case the width of the line was set at 25 μm and the first five terms of the basis function expansions for the currents were used. As can be seen from Fig. 5, the agreement between all three cases was excellent. The slight differences were attributed to the small discrepancies of the geometries, to the experimental accuracy, and to numerical limitations. In all cases presented, the quantity b/w was chosen so there was minimal sensitivity on the propagation coefficient.

The above case demonstrates the validity of the numerical formulation that has been developed. The correlation of the analytical and numerical results for geometries which are not as severe with respect to the width-to-height ratio was also good but, as expected, deteriorated as the width-to-height ratio approached unity. When the dielectric thickness of the suspended stripline was increased to 4.5 μm (a factor of 100 increase) a situation existed where the kinetic inductance contribution was of the same order as the magnetic inductance contribution. Values of Re(a)

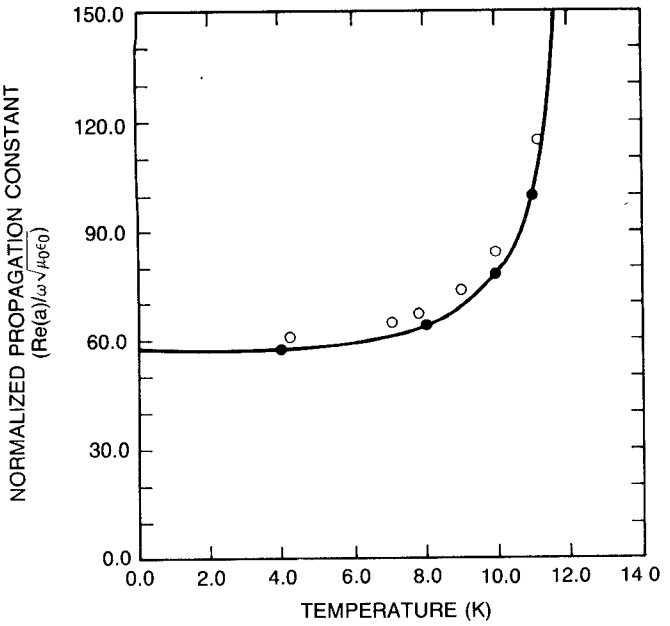

Fig. 5. A comparison of the experimental (∘), numerical (•), and analytical (———) results as a function of temperature is shown for geometries which most closely approximate the experimental case. The value of b/w is 4.0.

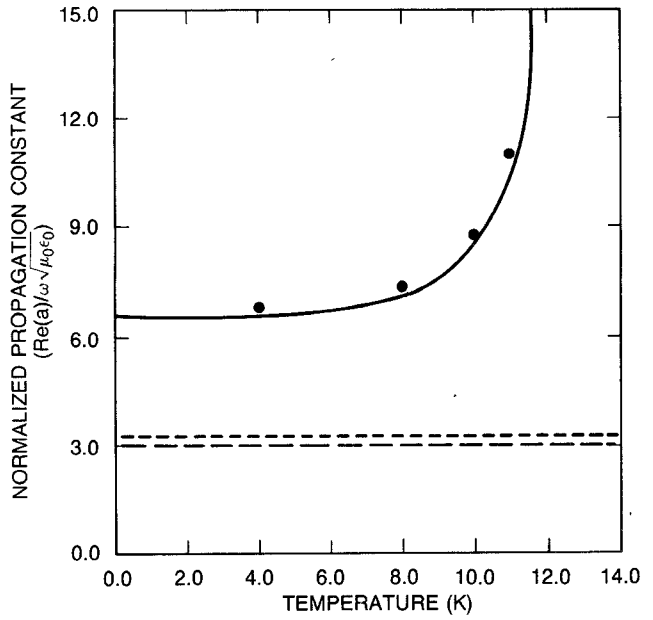

Fig. 6. A temperature-dependent comparison of the real part of the propagation coefficient is shown between the numerical solutions for superconducting stripline (•) and perfectly conducting stripline (— — — —). The strip is 25 μm wide, the dielectric thickness is 4.5 μm, and b/w is 4.0. Also plotted are the analytical solutions to the superconducting (———) and perfectly conducting (----) parallel-plate cases.

versus temperature for this case are shown in Fig. 6 at 1.0 GHz. The analytical parallel-plate results are compared to the numerical results using five terms of the basis function expansion. The agreement was within a few percent even in this case, where the width-to-height ratio (about 5.5) is not nearly as severe. In situations where the width-to-height ratio is not too large, there usually exist some fringing

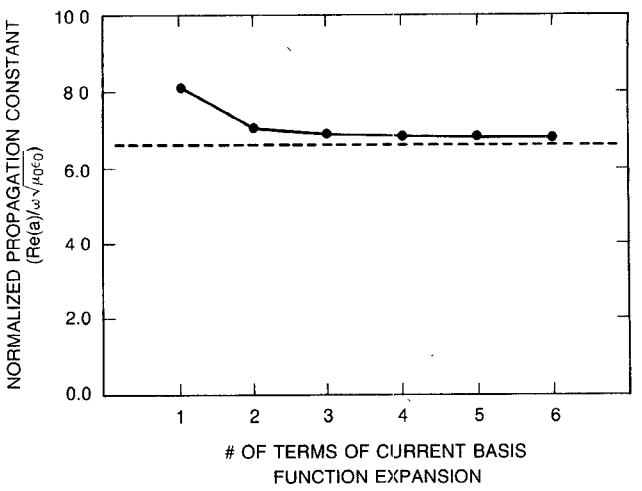

Fig. 7. The monotonic convergence (•) of the numerical solution is plotted as the number of terms of the basis function expansion is increased and approaches but does not converge to the analytical parallel-plate solution (— — —). The b/w value is 4.0.

fields which tend to be influenced by the lower value of the relative permittivity of dielectric layer above the strip. This usually results in a lower value of Re(a) than would otherwise be expected when compared to the parallel-plate situation. Interestingly, the numerical values of Re(a) were slightly higher than the analytical prediction. It is possible that this phenomenon was due to the singular behavior of the currents at the edge of the strip, which may increase the kinetic inductance contribution over that predicted by the analytical solution and result in a larger value of Re(a). For comparison purposes, the numerical solution for a perfectly conducting strip at 1.0 GHz and the analytical solution for a perfectly conducting parallel-plate waveguide are also plotted in Fig. 6. It can be seen that the propagation constant for the strip is less than the parallel-plate case, as would be expected from the fringing field behavior and the lower relative dielectric constant of the medium above the strip.

A study of the convergence of the numerical solution as a function of the number of terms of the basis function expansion has been undertaken. Results, shown in Fig. 7, demonstrate that the solution monotonically approaches the value predicted by the analytical parallel-plate model. The particular case presented here used the same geometry and film parameters as the case presented in the above paragraph, although other cases behaved similarly. In all situations examined to date, the convergence has occurred within four to six terms of the current basis function expansion. Using more than six terms yields no further improvement and sometimes, if the number of basis function terms exceeds about ten, the solution can diverge. This is attributed to accumulated numerical errors.

As another example, the results at 1.0 GHz of a geometry where the width-to-height ratio is approximately unity are presented in Fig. 8. The dielectric thickness and film parameters were kept the same as in the previous case, but the width of the strip was reduced to 5 μm. Convergence behavior was similar to that of the earlier cases. As the

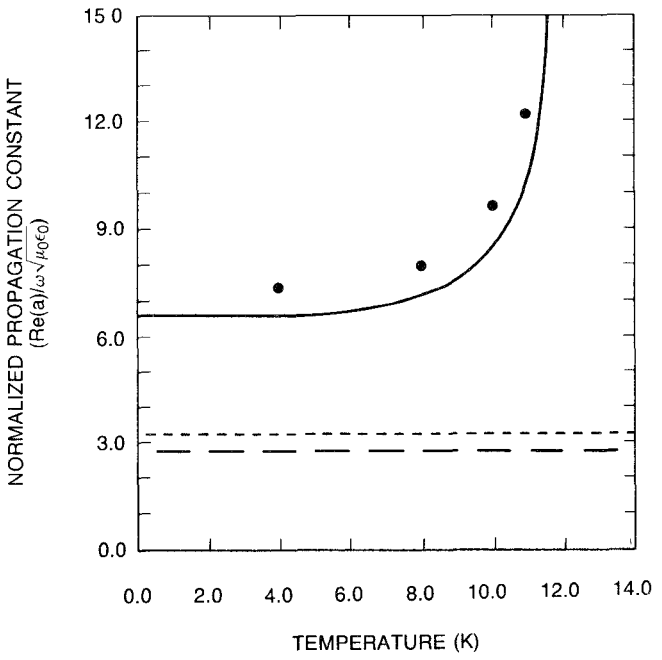

Fig. 8. A temperature-dependent comparison of the real part of the propagation coefficient is shown between the numerical solutions for superconducting stripline (•) and perfectly conducting stripline (———). The strip width is 5 μm, the dielectric thickness is 4.5 μm, and the b/w value is 20.0. Also plotted are the analytical solutions to the superconductng (— — — —) and perfectly conducting (----) parallel-plate cases.

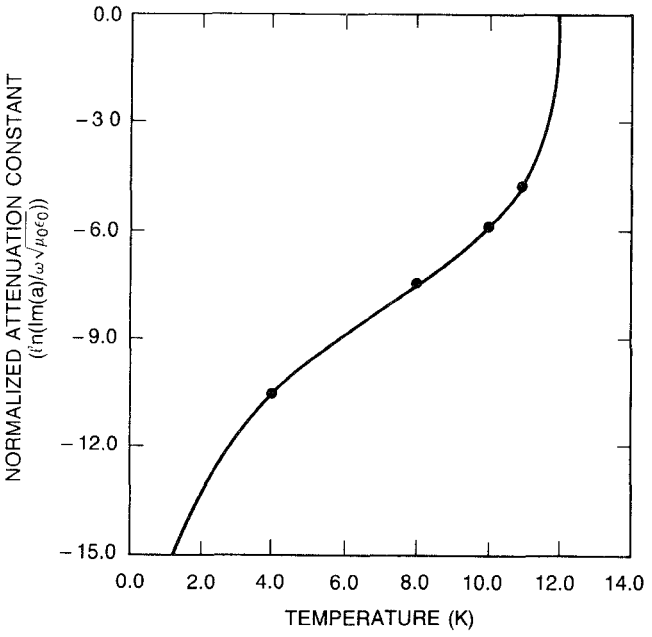

Fig. 9. The temperature dependence of the superconducting losses (ln[Im(a)]) is plotted to compare the analytical predictions using the parallel-plate waveguide (———) and the numerical results (•) from the suspended stripline case. The two-fluid model for complex conductivity was used. The strip width was 25 μm, the dielectric thickness was 4.5 μm, and the b/w value is 4.0. The value of σ_{nc} was chosen to be 1×10^{6} $(\Omega\cdot\mathrm{m})^{-1}$ and the dielectric loss was set to zero.

width of the strip decreased the accuracy of the parallel-plate model was expected to decrease. Indeed, this was the case, as can be seen in Fig. 8. Numerical results for the stripline predict a propagation constant about 12 percent larger than that predicted by the parallel-plate model. A comparison can be made to the perfectly conducting situations, which are also shown in Fig. 8. As before, the numerical value for the superconducting strip, rather than being smaller than the parallel-plate prediction due to fringing fields, was larger than the parallel-plate prediction. This was in contrast to the perfectly conducting cases, where the propagation constant of the strip was less than that for the parallel-plate waveguide. Such behavior was even more pronounced than in the case shown in Fig. 7. This was attributed to a greater percentage of the currents being in the singular regions at the edges of the strip for a narrower strip. As expected, the numerical results were virtually unchanged from 0.5 to 5.0 GHz.

Superconducting losses were also calculated and the agreement with the parallel-plate theory was good. In the cases considered so far, the dielectric loss was dominant since this was the limiting loss mechanism from the experimental results. In an artificial case, that of no dielectric loss, the behavior of the superconducting loss as a function of temperature was determined numerically and is shown in Fig. 9. Also shown is the theoretical behavior of Im(a) versus temperature for the parallel-plate case using (34). The agreement between the finite width and infinite width cases was very good. Except for the loss terms, the film parameters and geometry were the same as those described above to calculate the curves of Fig. 6. The strong dependence of the loss on T as $T\rightarrow T_c$ can be expected from (A2) and (A3).

VII. Conclusions

A novel use of the resistive boundary condition in the solution of electromagnetic transmission and scattering problems involving thin superconducting films has been presented. The solution to the parallel-plate waveguide problem was presented and was shown to agree with the solution using more traditional approaches. The use of this boundary condition leads to a modification in the Fourier-transformed coupled integral equation formulation of planar transmission line problems. The Fourier-transformed dyadic impedance Green's function of the coupled integral equations was modified by the complex resistive boundary condition. To document the power of this approach, the microstrip problem was solved numerically using the Galerkin method. Comparisons between the analytical, numerical, and theoretical results showed excellent agreement.

The boundary condition and numerical formulation presented in this paper are also applicable to slotline, coplanar stripline, and coplanar waveguide, where conventional approaches are inadequate since they are unable to treat the diaphanous nature of the thin superconductor. Since the propagation constants of these transmission lines are variable with temperature (and, in principle, electronically), they have many potential uses as microwave components such as tunable filters and variable phase shifters. Future work will focus on determining the propagation properties of these transmission lines in addition to microstrip.

APPENDIX

There exist several sets of expressions to describe the complex conductivity of a superconductor. Several of these are phenomenological including the two-fluid models of Gorter and Casimir and the Ginzburg–Landau model [9]. The two-fluid model will be emphasized in this paper since it is a good model for the observed behavior of the superconducting thin films used in the experimental part of the work. The Ginzburg–Landau model is applicable for T very close to but less than T_c, but this is less useful since the transmission structures of interest become quite lossy at these temperatures. The BCS derived model for complex conductivity of Mattis and Bardeen is theoretically based and can be applied to both local and nonlocal superconductors. Any of these particular models for complex conductivity can be used to calculate the resistive boundary condition.

In the two-fluid model, λ can be related to the density of the super electrons by

$$\lambda^2 = m/\left(e^2 n_{sc}\mu_0\right) \tag{A1}$$

with n_{sc} being the density of the superconducting electrons. The temperature dependencies of the conductivities for the two-fluid model are given by [9] from the temperature dependencies of the normal and super electron densities:

$$\sigma_n = \sigma_{nc}(T/T_c)^4 \tag{A2}$$

and

$$\sigma_{sc} = \left[1-(T/T_c)^4\right]\Big/\left(\omega\mu_0\lambda_0^2\right) \tag{A3}$$

where σ_{nc} is the conductivity just above the critical temperature, T_c, and λ_0 is the penetration depth at 0.0 K. A more accurate model, using the BCS derived conductivity [19], gives

$$\begin{aligned}\frac{\sigma_n}{\sigma_{nc}} = {} & \frac{2}{\hbar\omega}\int_{\Delta}^{\infty} dE\left[F(E)-F(E+\hbar\omega)\right] \\ & \cdot\frac{E^2+\Delta^2+\hbar\omega E}{\left(E^2-\Delta^2\right)^{1/2}\left[(E+\hbar\omega)^2-\Delta^2\right]^{1/2}} \\ & + \frac{1}{\hbar\omega}\int_{\Delta}^{\hbar\omega-\Delta} dE\left[1-2F(\hbar\omega-E)\right] \\ & \cdot\frac{\hbar\omega E-E^2-\Delta^2}{\left(E^2-\Delta^2\right)^{1/2}\left[(\hbar\omega-E)^2-\Delta^2\right]^{1/2}}\end{aligned} \tag{A4}$$

$$\begin{aligned}\frac{\sigma_{sc}}{\sigma_{nc}} = {} & \frac{1}{\hbar\omega}\int_{\Delta-\hbar\omega,\,-\Delta}^{\Delta} dE\left[1-2F(E+\hbar\omega)\right] \\ & \cdot\frac{E^2+\Delta^2+\hbar\omega E}{\left(\Delta^2-E^2\right)^{1/2}\left[(E+\hbar\omega)^2-\Delta^2\right]^{1/2}}\end{aligned} \tag{A5}$$

where

$$F(E) = \left[1+\exp(E/kT)\right]^{-1} \tag{A6}$$

and $\Delta = \Delta(T)$ is the energy gap parameter. The second integral of (A4) is zero when $\hbar\omega < 2\Delta$. The lower limit of (A5) becomes $-\Delta$ when $\hbar\omega > 2\Delta$. The relationship between the two theories can be established by noting [20] that for the local theory

$$\lambda = \lim_{\omega\to 0}\left(j\omega\mu_0\sigma\right)^{-1/2}. \tag{A7}$$

By choosing λ_0, $\Delta_0 = \Delta(T=0)$, and σ_{nc} to satisfy

$$\lambda_0 = \left[\hbar/(\pi\mu_0\sigma_{nc}\Delta_0)\right]^{1/2} \tag{A8}$$

the two-fluid model and the Mattis–Bardeen theory can be compared.

ACKNOWLEDGMENT

The authors thank Dr. D. Webb, Dr. E. Cukauskas, and Dr. M. Nisenoff for their comments.

REFERENCES

[1] S. A. Reible, "Wideband analog signal processing with superconductive circuits," in *1982 IEEE Ultrasonics Symp. Proc.* (San Diego, CA), Oct. 1982, pp. 190–201.

[2] A. B. Pippard, "The surface impedance of superconductor and normal metals at high frequencies—III: The relationship between impedance and superconducting penetration depth," *Proc. Roy. Soc. London*, vol. A191, pp. 399–415, 1947.

[3] J. M. Pond, J. H. Claassen, and W. L. Carter, "Kinetic inductance microstrip delay lines," *IEEE Trans. Magn.*, vol. MAG-23, pp. 903–907, Mar. 1987.

[4] J. M. Pond, J. H. Claassen, and W. L. Carter, "Measurements and modeling of kinetic inductance microstrip delay lines," *IEEE Trans. Microwave Theory Tech.*, vol. MTT-35, pp. 1256–1262, Dec. 1987.

[5] W. H. Henkels and C. J. Kircher, "Penetration depth measurements on type II superconducting films," *IEEE Trans. Magn.*, vol. MAG-13, pp. 63–66, Jan. 1977.

[6] C. S. Owen and D. J. Scalapino, "Inductive coupling of Josephson junctions to external circuits," *J. Appl. Phys.*, vol. 41, pp. 2047–2056, 1970.

[7] K. Yoshida, T. Nagatsuma, S. Kumataka, and K. Enpuku, "Millimeter-wave emission from Josephson oscillator through thin film junction electrode," *IEEE Trans. Magn.*, vol. MAG-23, pp. 1283–1286, Mar. 1987.

[8] T. B. A. Senior, "Half plane edge diffraction," *Radio Sci.*, vol. 10, pp. 645–650, June 1975.

[9] T. VanDuzer and C. W. Turner, *Principles of Superconductive Devices and Circuits*. New York: Elsevier, 1981.

[10] R. Meservey and P. M. Tedrow, "Measurements of the kinetic inductance of superconducting linear structures," *J. Appl. Phys.*, vol. 40, pp. 2028–2034, Apr. 1969.

[11] J. C. Swihart, "Field solution for a thin-film superconducting strip transmission line," *J. Appl. Phys.*, vol. 32, pp. 461–469, Mar. 1961.

[12] P. V. Mason and R. W. Gould, "Slow-wave structures utilizing superconducting thin film transmission lines," *J. Appl. Phys.*, vol. 40, pp. 2039–2051, Apr. 1969.

[13] T. Itoh and R. Mittra, "Spectral-domain approach for calculating the dispersion characteristics of microstrip lines," *IEEE Trans. Microwave Theory Tech.*, vol. MTT-21, pp. 496–499, July 1973.

[14] T. Itoh, "Spectral-domain immittance approach for dispersion characteristics of generalized printed transmission," *IEEE Trans. Microwave Theory Tech.*, vol. MTT-28, pp. 733–736, July 1980.

[15] A. A. Mostafa, C. M. Krowne, and K. A. Zaki, "Numerical spectral matrix method for propagation in general layered media: Application to isotropic and anisotropic substrates," *IEEE Trans. Microwave Theory Tech.*, vol. MTT-35, pp. 1399–1407, Dec. 1987.

[16] C. M. Krowne, "Slow wave propagation in generalized cylindrical waveguides loaded with a semiconductor," *Int. J. Electron.*, vol. 58, pp. 249–269, Feb. 1985.

[17] R. E. Matick, *Transmission Lines for Digital and Communication Networks*. New York: McGraw-Hill, 1969, ch. 6.

[18] C. T. Tai, *Dyadic Green's Functions in Electromagnetic Theory*. Scranton, PA: Intext, 1971.

[19] D. C. Mattis and J. Bardeen, "Theory of the anomalous skin effect in normal and superconducting metals," *Phys. Rev.*, vol. 111, pp. 412–417, 1958.

[20] R. L. Kautz, "Picosecond pulses on superconducting striplines," *J. Appl. Phys.*, vol. 49, pp. 308–314, Jan. 1978.

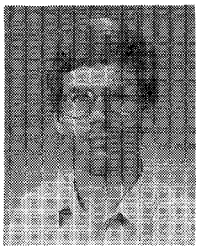

Jeffrey M. Pond (S'82–M'82) was born in South Haven, MI, in 1956. He received the B.S. degree in electrical engineering from Michigan State University in 1978 and the M.S. and Ph.D. degrees in electrical engineering from the University of Michigan in 1979 and 1982, respectively.

In 1982 he joined the Naval Research Laboratory in Washington, DC. His research interests have centered on semiconductor and superconductor devices and circuits for microwave applications.

✠

Clifford M. Krowne (S'73–M'74–SM'84) attended the University of California, Berkeley, and received the B.S. degree in physics from the University of California, Davis, in 1970 and the M.S. and Ph.D. degrees in electrical engineering from the University of California, Los Angeles, in 1972 and 1975, respectively.

In 1970, he was employed in the Microelectronics Division of Lockheed Missiles and Space Company. In 1975 he joined the technical staff of the Watkins-Johnson Company in Palo Alto, CA, and in 1978 he became a faculty member of the Department of Electrical Engineering at North Carolina State University, Raleigh. He has been a consultant to several industrial firms and was a 1980 ASEE Summer Faculty Fellow at the NASA Johnson Space Center, Houston, TX. Since 1981, he has been with the Electronics Technology Division of the Naval Research Laboratory, Washington, DC, studying microwave and millimeter-wave properties of active and passive solid-state devices. He is also an adjunct professor of electrical engineering at the University of Maryland, College Park.

Dr. Krowne has published more than 80 technical papers in solid-state electronics, microwave circuits, electromagnetics, and engineering education. He has served on the technical program conference committees of the Antennas and Propagation Society and the Microwave Theory and Techniques Society and chaired sessions in the electromagnetic theory, microstrip antenna, and solid-state devices/circuits areas. Dr. Krowne is a member of Phi Kappa Phi, Tau Beta Pi, the American Physical Society, and the New York Academy of Sciences.

✠

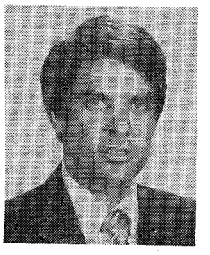

William L. Carter was born in Lynn, MA, on December 4, 1953. He received the B.A. degree from Carleton College in 1976 and the Ph.D. degree in physics from Stanford University in 1983.

In 1983 he joined the U.S. Naval Research Laboratory Electronics Technology Division, where he worked on thin-film growth and thermal processing of advanced superconducting materials and devices for use in microwave and millimeter-wave components. Since June 1988 he has been employed as a Senior Scientist in the Development Group at American Superconductor, Cambridge, MA.